Experimental set-up for the validation of numerical methods in electromagnetic dosimetry

D. Giordano[1], L. Zilberti[1], M. Borsero[1], R. Forastiere[2], W. Wang[1]

[1] INRIM, strada delle Cacce 91 – 10135 Torino, d.giordano@inrim.it, l.zilberti@inrim.it, m.borsero@inrim.it
w.wang@inrim.it
[2] Dip. Energia, Politecnico di Torino, corso Duca degli Abruzzi – 10129 Torino,
roberto.forastiere@studenti.polito.it

Abstract- One of the scientific challenges in the electromagnetic compatibility (EMC) and electromagnetic field exposure area is the validation, by means of suitable experiments, of the numerical procedure aimed at the estimation of the electromagnetic quantities generated in a test volume or induced in a human body [1, 2]. This paper describes the arrangement of a first experimental set-up which will allow to compare the measurement of the electromagnetic field quantities induced inside a simple cylindrical phantom with the same quantities estimated numerically.

I. Introduction

An estimated 8 – 10% of the European population are carrying medical implants. At present, they are excluded from receiving a Magnetic Resonance Imaging (MRI) scan as no metrics exists to assess the specific safety risks related to these implants.

With the aim of investigating implant associated risks, advanced modelling concepts for the evaluation of electromagnetic field inside phantoms and human computer models [3] are fundamental tools which must be validated by experimental comparisons to guarantee their reliability. To this end an experimental tool was designed and set up and first comparisons between measurements and numerical results obtained through a Boundary Element Method (BEM) algorithm, are presented in the paper.

Since this preliminary investigation is based on a simple numerical model involving all the physical aspects, a simplified experimental tool is required as well. To do that a system made of a cylindrical phantom with a human-tissue liquid, a loop antenna and a 3D electromagnetic field mapping was set up.

The magnetic source and measuring system shall be able to generate and detect Radio Frequency (RF) electromagnetic fields with magnitude and frequency similar to the ones exploited by Magnetic Resonance Imaging (MRI) devices for diagnostic purposes. As regards the frequency, it shall be comparable with the isocenter resonance frequency (Larmor frequency) of the most used MRI devices. These are characterized by frequencies of about 64 MHz, 128 MHz and 300 MHz related to isocenter static magnetic fields of 1.5 T, 3 T and 7 T respectively. For these preliminary investigations the frequency range of interest was up to 70 MHz [3].

As well known from the Nuclear Magnetic Resonance (NMR) theory, a rotation of the nuclear magnetic moment vectors can be impressed by transferring a suitable amount of energy into the anatomy by means of coils tuned at the Larmor frequency. Such coils have to generate just magnetic fields perpendicular to the static magnetic field direction. Consequently, a loop antenna was selected.

Since the aim of this paper is essentially relating to the experimental set-up, just a synthetic description of the field formulation is given in section II.

In section III a description of the experimental set-up is given, and some critical items due to the simplified model of the loop antenna are pointed out. In particular, the shield covering the actual loop and the absence of the earth in the numerical model are argued.

The first comparisons between measured and computed magnetic field components were performed along a vertical and a horizontal line inside the cylindrical phantom, as shown in section IV.

II. Field formulation

The electromagnetic field problem is described by the Electric Field Integral Equation (EFIE) and Magnetic Field Integral Equation (MFIE) under sinusoidal conditions (angular frequency ω). The integral equations are solved by the Boundary Element Method, discretizing the external surface of the phantom with 2-D surface elements. The discretized form the the EFIE and MFIE equations are:

19th Symposium IMEKO TC 4 Symposium and 17th IWADC Workshop
Advances in Instrumentation and Sensors Interoperability
July 18-19, 2013, Barcelona, Spain

$$\xi \boldsymbol{E}_i = -\int_{\Omega_s} j\omega\mu\Psi\boldsymbol{J}_s dv - \sum_m^M (\boldsymbol{n}\times\boldsymbol{E})_m \times \int_{\partial\Omega_m} \nabla\Psi_{i,m} ds \qquad \xi \boldsymbol{H}_i = \int_{\Omega_s} (\boldsymbol{J}_s\times\nabla\Psi) dv - \sum_m^M (\boldsymbol{n}\times\boldsymbol{H})_m \times \int_{\partial\Omega_m} \nabla\Psi_{i,m} ds$$

$$-\sum_m^M (\boldsymbol{n}\cdot\boldsymbol{E})_m \int_{\partial\Omega_m} \nabla\Psi_{i,m} ds + j\omega\mu\sum_m^M (\boldsymbol{n}\times\boldsymbol{H})_m \int_{\partial\Omega_m} \Psi_{i,m} ds \qquad -\sum_m^M (\boldsymbol{n}\cdot\boldsymbol{H})_m \int_{\partial\Omega_m} \nabla\Psi_{i,m} ds - j\omega\tilde\varepsilon\sum_m^M (\boldsymbol{n}\times\boldsymbol{E})_m \int_{\partial\Omega_m} \Psi_{i,m} ds \qquad (1)$$

where J_s is the impressed current density of the sources, ξ is the singularity factor ($\xi = 0.5$ on the surface and $\xi = 1$ elsewhere) and n is the normal unit vector directed outwards Ω. The *m-th* element is the source point while, during the setting of the matrix, the computational point is the barycentre of the *i-th* element. The Green function is defined as:

$$\Psi = \frac{e^{-ik|r-r'|}}{4\pi|r-r'|} \quad \text{with} \ k = \omega\sqrt{\mu\left(\varepsilon - j\frac{\sigma}{\omega}\right)} = \omega\sqrt{\mu\tilde\varepsilon} \qquad (2)$$

where r and r' are the coordinate vectors of the observation and of the source points, while μ, σ and ε are the magnetic permeability, the electric conductivity and the electric permittivity respectively.
The integrals of the Green function and its gradient are computed by using an adaptive quadrature rule based on Kronrod algorithm, which enables high accuracy limiting the computational burden.

III. Experimental set-up

Figure 1 shows an overall view of the experimental set-up, including the phantom filled with a yellow liquid (the human tissue-like liquid), the 3D probe positioning system made of dielectric material with low permittivity ($\varepsilon_r = 2$), the electric (or magnetic) field probe and its optical converter, the support for the antennas (more antennas are foreseen). The black loop antenna can be seen on the right side of the phantom.
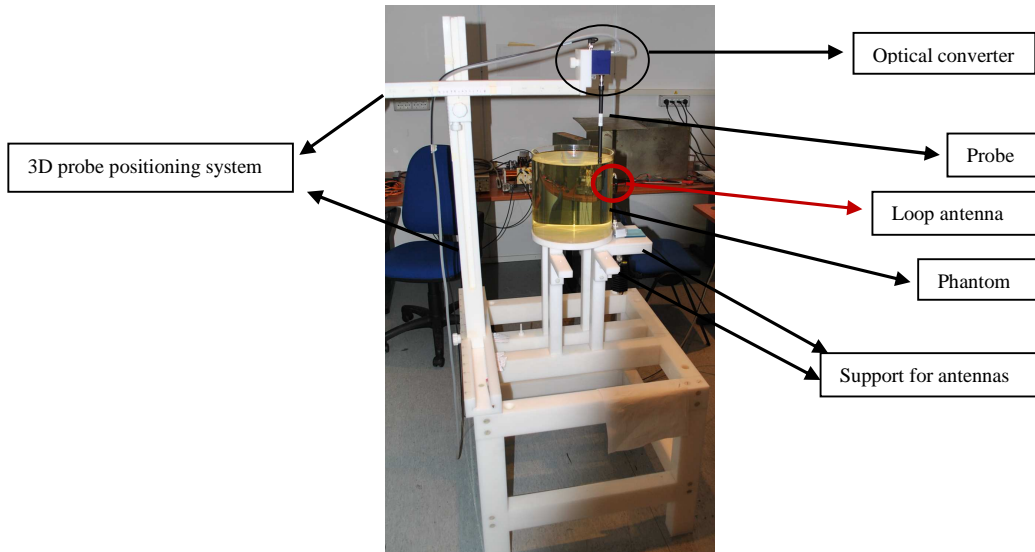

Figure 1. Experimental set-up

A. Phantom

The phantom consists of a cylindrical container (Figure 2 a) made of polymethylmethacrylate whose dielectric permittivity ($\varepsilon_r = 2,2$), much lower than that of the liquid, does not affect the electric field induced in the phantom. The cylindrical geometry is selected to reduce the burden of the numerical simulation. It has both an internal diameter and an internal height equal to 240 mm. The liquid, prepared by the Physikalisch Technische Bundesanstalt laboratories (PTB, Berlin), shows electrical characteristics comparable with human tissues. Figure 2 b) and c) shows the electric permittivity and conductivity versus frequency for different temperature values.
To reduce the effects of the support material on the electric field behavior around the phantom, four slim columns sustain the container increasing the distance from the structure supporting the whole system.

19th Symposium IMEKO TC 4 Symposium and 17th IWADC Workshop
Advances in Instrumentation and Sensors Interoperability
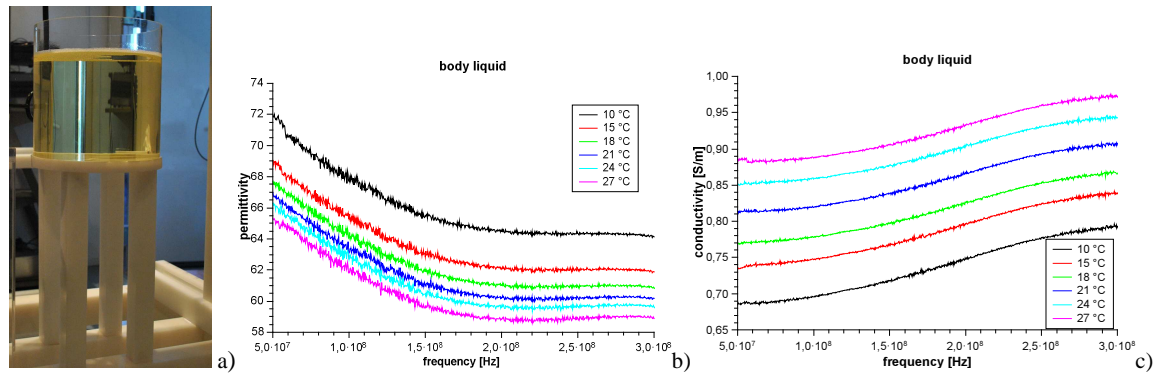July 18-19, 2013, Barcelona, Spain

Figure 2. Phantom filled with human tissue-like liquid a) frequency behaviour of liquid permittivity b) and conductivity c) at different temperatures.

B. Magnetic field generation system

The magnetic field source shall be able to induce, inside the phantom, an electric field with a magnitude detectable by the near-field probes employed for this experiment. Moreover, the source should not produce spurious electric fields which are not considered in the numerical procedure.

The selected source for these purposes is a small loop antenna, consisting of a single turn of 6 cm diameter, inside a balanced E-field shield (Figure 3a).

Through preliminary computations, a magnetic field amplitude equal to 1 A/m obtained by a current of 0.5 A is predicted at 20 mm far from the loop. This value is of course lower than the typical magnetic field value generated by the RF imaging coil of the MRI devices [4]; nevertheless, this is acceptable because the purpose here is not to cause the nuclear magnetic resonance but to investigate the possible side-effects induced in the human body during MRI examination. The estimated electric field induced by such magnetic field is a few tens of volts per meter, enough to be detected by the probe.
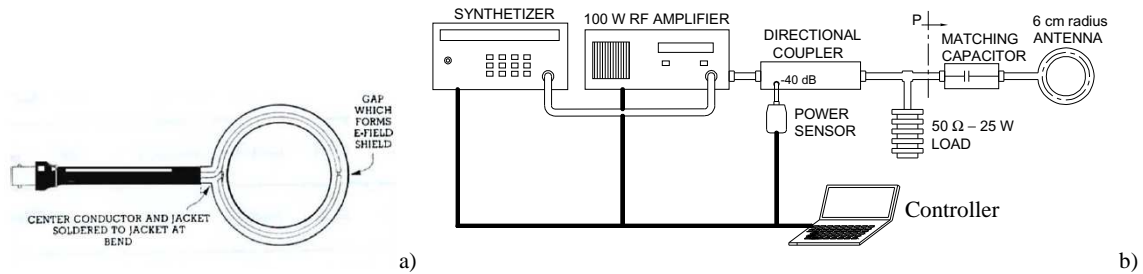

Figure 3. Sketch of the loop antenna a); sketch of the set-up for the generation of RF magnetic field b)

A first experimental arrangement for the supply and estimation of the current flowing in the antenna is depicted in Figure 3 b). The supply system consists of a synthesizer and a 100 W broadband amplifier (9 kHz to 100 MHz). In order to improve the matching between the supply system and the antenna, a series capacitor C_s, with a rated value of 8 pF, is introduced. In this way it is possible to obtain the required field without exceeding the maximum power (25 W) of the 50 Ω resistive load. This load allows to estimate the current which generates the field. Indeed, through the knowledge of the voltage across the resistive load, obtained by the measurement of the incident power P, it is possible to solve the circuital model shown in Figure 4a and estimate the current that flows in the inductance L simulating the loop antenna. The parameter C_L simulates the stray electrical coupling between the loop wire and its shield. Because of the antenna dimensions and supply frequency, the radiation resistance can be neglected as well as the Joule losses and the circuital model can be simplified.

The current flowing in the loop antenna (thus in the inductance L), I_L, which generates the magnetic field, can be directly estimated by knowing the transmitted power to R_{Load} and the admittance T defined as:

$$|\overline{T}| = \frac{|\overline{I_L}|}{|\overline{V_f}|} = \frac{\omega \cdot C_s}{1 - \left(\dfrac{\omega}{\omega_{res}}\right)^2} \qquad \text{with} \qquad \omega_{res} = \frac{1}{\sqrt{L \cdot (C_L + C_s)}} \qquad (3)$$

The transmitted power is obtained as difference between the incident and reflected power values measured by means of a directional coupler and a power meter. From that, the voltage V_f is easily obtained.

The unknown C_s and ω_{res} are extrapolated from the experimental frequency behavior of T from 45 MHz to 70 MHz by means of a least square algorithm between the measured frequency behavior and the computed one.

Assuming that the current is uniform along the single turn (i.e., $\pi D < \lambda/10$, where D is the turn diameter and λ is the wavelength of the working frequency), the magnetic field in the loop center is $H_c = \dfrac{I_L}{D}$; then the following system can be written:

$$\begin{cases} \left|\overline{T}\right|(\omega_1) = D\left.\dfrac{H_c}{\left|\overline{V}_f\right|}\right|_{\omega_1} = \dfrac{\omega_1 \cdot C_s}{1-\left(\dfrac{\omega_1}{\omega_{res}}\right)^2} \\[3em] \left|\overline{T}\right|(\omega_2) = D\left.\dfrac{H_c}{\left|\overline{V}_f\right|}\right|_{\omega_2} = \dfrac{\omega_2 \cdot C_s}{1-\left(\dfrac{\omega_2}{\omega_{res}}\right)^2} \end{cases} \tag{4}$$

where ω_1 and ω_2 are arbitrary angular frequencies chosen in the range 45 MHz to 70 MHz. From a series of measured values $\dfrac{H_c}{V_f}(\omega_i)$ evaluated in the same frequency range it is randomly extracted a couple of such values to solve the system (4) obtaining a series of couple of values ($C_{s\text{-I}}$, $\omega_{res\text{-i}}$). By means of the above cited least square algorithm between the measured $T(\omega)$ values and the computed ones the optimal couple of values (C_s, ω_{res}) were found to be equal to 8,3 pF and 70,6 MHz, respectively. Figure 4b shows the frequency behaviour of the computed and measured T coefficient.
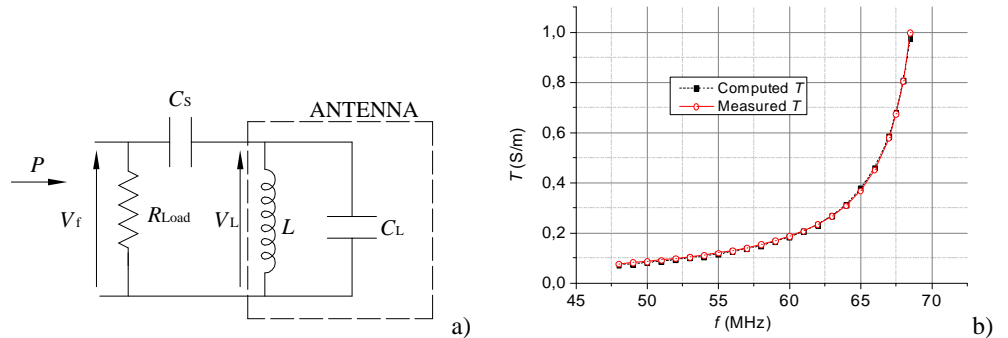

Figure 4. a) Circuital model for the estimation of the current flowing in the loop antenna. b) Computed and measured frequency behaviour of T coefficient.

The gap on the E-field shield such as a coupling between the antenna and earth, due to a non-symmetric supply, can compromise the comparison between measurement and numerical results. Indeed the two elements introduce spurious electric components which are not taken into account by the numerical procedure. A non symmetric supply for the antenna generates a common electric coupling with the earth evidenced by a earth parallel electric field component which is not foreseen by the model. The gap problem can be overcome by shielding the gap with a metallic strip. The earth coupling disappears when the antenna is placed close to the phantom. The conductivity of the liquid "shields" the antenna from the earth. The encouraging results shown in the following prove the reliability of the assertions.

C. Electric and magnetic field probes

Since the electromagnetic field measurement should be performed in the near-field region, probes with very small dimensions are chosen. Moreover, owing to their usage inside the phantom, resistance to organic solvent must be guaranteed. Their main characteristics are resumed in Table I.

These isotropic probes give the true rms value of the applied field along the three orthogonal axes. Thanks to an electro-optic converter the information can be easily carried from the probe to the meter which can be placed a few meters away from the magnetic source.

The field generation and detection system is automatically managed by a Python program which reduces the measurement time and increases the accuracy of the power measurement which requires to reach a thermal equilibrium.

19th Symposium IMEKO TC 4 Symposium and 17th IWADC Workshop
Advances in Instrumentation and Sensors Interoperability
July 18-19, 2013, Barcelona, Spain

Table I – Characteristics of the electric and magnetic field probes

	Electric field	**Magnetic Field**
Frequency	40 MHz to 6 GHz	10 MHz to 600 MHz (absolute accuracy ± 6.0%); output linearized
Dynamic range	2 V/m to 1000 V/m	0.08 A/m to 40 A/m at 13.56 MHz 0.01 A/m to 5 A/m at 100 MHz
Overall length:	337 mm (tip: 40 mm)	337 mm (tip: 40 mm)
Distance from probe tip to dipole centre	2.5 mm	3 mm
Tip diameter	8 mm (body: 10 mm)	6 mm (body: 12 mm)

IV. Numerical model – measurement comparison

As first comparison between the BEM algorithm and measurements, two investigation lines were chosen. Line 1 is parallel to the y axis (Figure 5), 30 mm above it. Since the induced current effects on the magnetic field at 64 MHz are negligible, the ideal magnetic field array lies on y-z plane, so H_{x_BEM} component is null (Figure 6a). The electric field lines induced in the phantom are, at this frequency, circular with the centres on y axis, as depicted in Figure 5; thus, only E_{x_BEM} is not zero along the investigation line (Figure 6b).
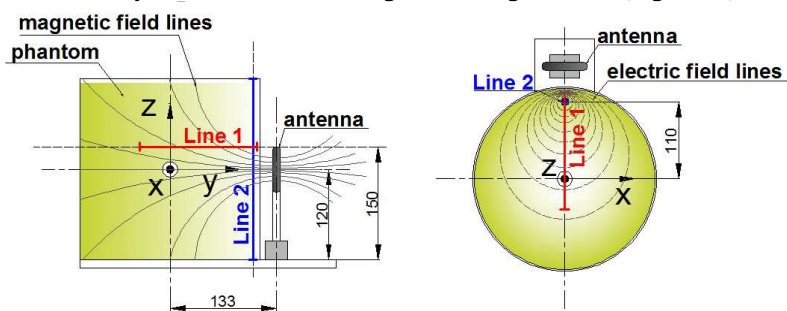

Figure 5 Investigation lines inside the phantom and a sketch of the ideal field lines: frontal and upper view.

Line 2 is parallel to z axis and is placed 110 mm from the reference system centre. Since this line lies on the z-y plane which cuts symmetrically the antenna, the H_{x_BEM} component is null, H_{z_BEM} shows two peaks (Figure 7a) in correspondence with the minimum distance between the line 2 and the turn of the antenna while H_{y_BEM} reaches the peak in correspondence with the loop antenna axis. The shape of the E_{x_BEM} component should be analogous to the shape of H_{z_BEM} while E_{y_BEM} and E_{z_BEM} are zero (Figure 7b) because of the circular shape of the electric field lines.

When performing electric field measurements the noise level was not always negligible (in the order of 2 to 3 V/m). To reduce the noise effects on the measured values, the following expression was employed:

$$E_{64MHz} = \sqrt{E_{tot}^{2} - E_{noise}^{2}} \tag{5}$$

where E_{64MHz} is the electric field corrected for the noise, E_{tot} is the electric field given by the meter (signal plus noise) and E_{noise} is the mean value of the noise detected when the loop antenna is not supplied.

The magnetic and electric field behaviours shown in Figure 6 and Figure 7 are obtained by imposing a per unit-current (1 A) flowing in the loop antenna.

The measured magnetic field on both lines satisfactorily follows the theoretical behavior, The electric field component E_{y_MEAS}, which should be zero, appears with a shape similar to E_{x_MEAS}. This means that an offset of the actual lines along x axis was introduced, the error positioning error is found to be one of the main sources of uncertainty in the measurement.
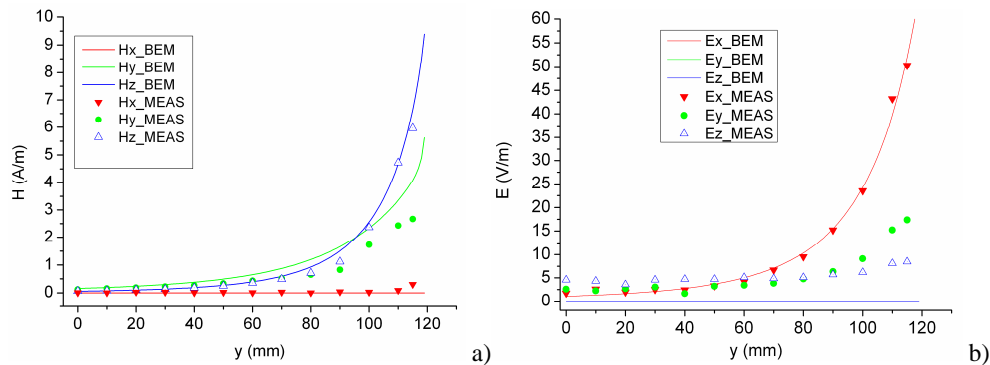
Figure 6. Magnetic a) and electric b) r.m.s. field behaviour along line 1 of the three components with a unit-current in the antenna.
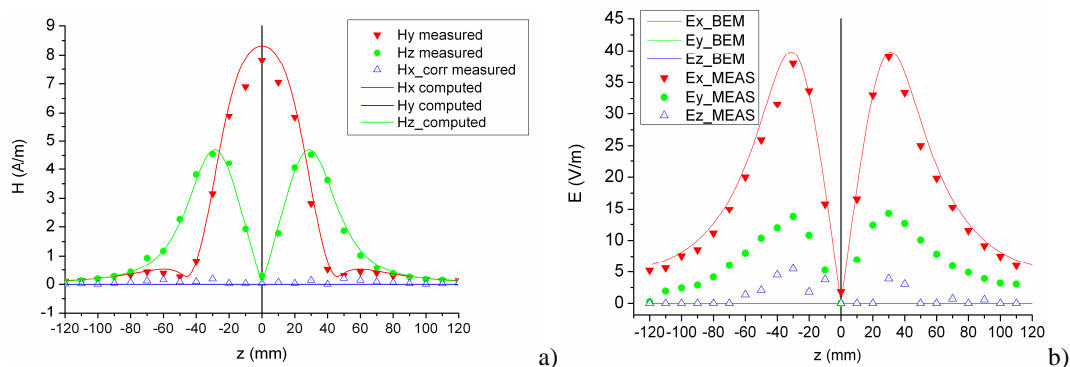

Figure 7. Magnetic a) and electric b) r.m.s. field behaviour along line 2 of the three components with a unit-current in the antenna.

V. Conclusions

A description of a first experimental set-up devoted to the assessment of the reliability of numerical models for the estimation of induced electromagnetic fields into a phantom simulating human tissues is presented. A simple model of the transmitter antenna with lumped parameters is implemented and an evidence of the effectiveness of the model is given up to about 70 MHz. A first comparison between computation and measurement along two investigation lines inside the phantom is shown. The results are encouraging, a probable misalignment was evidenced from the electric field measurement results. An improvement on the positioning system accuracy is in progress. The design of a new antenna system is being developed to increase the value of the magnetic field-strength generated in the phantom. The numerical approach reliability will be investigated in presence of metallic elements simulating medical implants.

References

[1] IEC 62311 "Assessment of electronic and electric equipment related to human exposure restrictions for electromagnetic fields (0 Hz – 300 GHz), 2007.

[2] M. Borsero, O. Bottauscio, L. Zilberti, M. Chiampi, W. Wang "A Boundary Element estimate of radiated emissions produced by unknown sources", Proc. of EMC Europe 2012, Rome, Sept. 2012.

[3] O. Bottauscio, M. Chiampi, L. Zilberti "Boundary element approach to relate surface fields with the specific absorption rate (SAR) induced in 3-D human phantoms", Eng. Analysis with Boundary Elements vol 35 (2011) pp. 657–666.

[4] Joseph P. Hornak "The Basics of MRI", www.cis.rit.edu/htbooks/mri/, 1996.

[5] Stefano Pisa, et all. "A study of the Interaction Between Implanted Pacemakers and the Radio-Frequency field Produced by Magnetic Resonance Imaging apparatus", IEEE Trans. on EMC, vol. 50, NO.1, pp. 35-42, February 2008.